

Global mapping of flux and microbial sources for oceanic N₂O

Received: 18 September 2024

Accepted: 31 March 2025

Published online: 08 April 2025

Shuo Wang^{1,4}, Jilin Huang^{1,4}, Zhen Wu^{1,2}, Shengjie Li³, Xianfang Zhu¹, Yong Liu¹✉ & Guodong Ji¹✉

The ocean is the largest source of N₂O emissions from global aquatic ecosystems. However, the N₂O production–consumption mechanism and microbial spatial distribution are still unclear. Our study established a bottom-up model based on the source–sink boundary and the microbial sources of N₂O. A high-resolution (0.1°) global distribution of oceanic N₂O was depicted, confirmed by approximately 150,000 surface measurements. The microbial N₂O flux is 2.9 Tg/yr N-N₂O, with the oxygen-deficient zones (ODZs) disproportionately accounting for more than half of the total emission. High primary productivity, sharp oxyclines, and shallow emission depths caused the ODZs to be N₂O hotspots. Geographically, ammonia-oxidizing archaea (AOA, 1.0 Tg) are the most widely distributed contributors to N₂O emissions in the ocean, completely overtaking ammonia-oxidizing bacteria (AOB). Heterotrophic denitrification, mainly occurring in ODZs, contributes the most (1.6 Tg) to N₂O emissions. Overall, this study offers a bottom-up framework for understanding microbial source-sink mechanism in the ocean.

Nitrous oxide (N₂O), one of the most important greenhouse gases and the greatest human-related threat to the ozone layer, has increased substantially, by over 23%, since preindustrial times¹. As a long-lived (116 ± 9 years) greenhouse gas, nitrous oxide (N₂O) is 265–298 times higher than CO₂ in the global warming potential on a 100-year timescale². Oceans are among Earth's largest sources of N₂O emissions, second only to natural soils and agriculture (IPCC). Although the amount of oceanic emissions has been well constrained^{3,4}, current estimates are usually based on air–sea flux (ΔpN₂O)^{3,5} or simple semi-empirical equations^{6–8}; thus, the N₂O production–consumption mechanism and spatial distribution of microbial N₂O sources in oxygen-stratified oceans are still unclear^{9,10}.

N₂O emissions are microbially driven and highly oxygen sensitive in the ocean, leading to high heterogeneity in ΔpN₂O. However, the coverage of ΔpN₂O data is generally limited and in broad ranges, uncertainties inevitably widen when extrapolating ΔpN₂O data to the global scale³. Moreover, sources and sinks coexist in the oxygen-

stratified ocean^{11–13}, and surface-based measurements cannot reflect the production and consumption of N₂O in the deep layers. Therefore, how N₂O is emitted from the ocean, how deep the source–sink boundary is, and how it evolves cannot be explained, especially under the effects of increased stratification and deoxygenation expansion¹⁴.

Most quantitative analyses of N₂O microbial sources are conducted at the regional scale^{11,12} or on the basis of semiempirical equations of nitrification and denitrification^{6–8,10}, which do not consider the niche separation of N₂O-related microbial processes in different ecological niches^{6–8}. For example, ammonia-oxidizing archaea (AOA) have greater affinity for substrates and compete for ammonia-oxidizing bacteria (AOB) in the NH₄⁺-limited ocean^{15,16}. Nevertheless, several studies have reported the contribution of AOB to marine N₂O emissions via nitrifier denitrification (NDN)¹⁷. Under hypoxic or anoxic conditions, N₂O is produced as an intermediate during heterotrophic denitrification (HDN), with organic matter as the electron donor^{10,18}. However, the quantification and spatial distributions of these

¹College of Environmental Sciences and Engineering, State Environmental Protection Key Laboratory of All Material Fluxes in River Ecosystems, Peking University, Beijing, China. ²Department of Earth, Atmospheric and Planetary Sciences, Massachusetts Institute of Technology, Cambridge, MA, USA.

³Department of Biogeochemistry, Max Planck Institute for Marine Microbiology, Bremen, Germany. ⁴These authors contributed equally: Shuo Wang, Jilin Huang. ✉ e-mail: yongliu@pku.edu.cn; jiguodong@pku.edu.cn

microbes with respect to N_2O emissions have not been well depicted in the ocean^{9,10}.

In this study, we established a bottom-up model based on the source–sink boundary and the microbial sources of marine N_2O . Extensive literature research has been conducted to obtain the geochemical profiles of DO and N_2O concentrations and isotopic signatures ($\delta^{15}\text{N}^{\text{Bulk}}$, $\delta^{18}\text{O}$ and $\delta^{15}\text{N}^{\text{SP}}$) at in situ locations (approximately 1000 lines of data), along with the isotopic characteristic values for each N_2O production pathway (i.e., AOA, AOB, HDN, and NDN). We identified the source–sink boundary of N_2O via global oxygen stratification (up to 5000 m) in the water column. FRAME model was then used to quantify the specific microbial contributions to N_2O emissions and N_2O reduction degree¹⁹. Finally, the ammonification (ammonia oxidation) flux, N_2O yield during ammonification ($\text{N}_2\text{O-N}/\text{NH}_4^+\text{-N}$), quantified N_2O microbial sources and fraction of residual unreduced N_2O ($r_{\text{N}_2\text{O}}$) were combined as constraints to accurately estimate global marine N_2O emissions. The results have been confirmed by a large compilation of N_2O in situ measurements (approximately 150,000)³. Overall, our results present a detailed spatial distribution of marine N_2O emissions with a source–sink mechanism and quantified microbial sources.

Results and discussion

N_2O source–sink boundary in the ocean

Due to the limit of light, the decomposition of organic matter or the poor mixing and ventilation, the ocean is oxygen-stratified. Earlier studies have revealed maximum N_2O concentration in the oxygen minimum zones of the ocean^{11,20,21}. N_2O has a perfect mirror-image relationship with DO and reaches its highest concentration at the lowest amount of dissolved oxygen (Supplementary Figs. 2–11)^{11,22}. Regardless of the upwelling, the source–sink boundary of N_2O , below which the water column does not contribute to N_2O emissions, was identified by a comprehensive grid-by-grid (0.1°) traversal of DO up to 5000 m in the ocean (Fig. 1). In oxygen-deficient zones (ODZs), DO decreases to anaerobic levels (minimum $\text{O}_2 \leq 10 \mu\text{M}$) at shallower depths (387.9 m on average, Fig. 1b). In addition to the three major ODZs (Fig. 1c), namely, the Eastern Tropical North Pacific (ETNP), Eastern Tropical South Pacific (ETSP), and Arabian Sea, we also found some sporadic ODZs in the North Pacific Ocean, indicating the potential hotspots of N_2O emissions. The upper oxycline (UO), with a N_2O peak at the oxic–anoxic interface (Supplementary Fig. 2–5), is the engine driving N_2O diffusion to the mixed layer (ML). The sharp oxycline creates favorable conditions for incomplete denitrification and nitrification with high N_2O yields, driving high supersaturation and fluxes of N_2O at the surface^{11,23}. Additionally, a stable proportionality of 0.45 and 2.58 for the plot of $\delta^{18}\text{O}$ versus $\delta^{15}\text{N}^{\text{Bulk}}$ ($R^2 = 0.52$, Supplementary Fig. 12) was observed above and below the source–sink boundary, respectively. In general, a strong correlation with slopes of 2.6 is evident when reduction process dominates, which contrasts from a slope of <1 commonly observed for mixing of N_2O production and atmospheric N_2O ^{24–26}. The slope of 0.45 proved the production, mixing and emission of N_2O in the source part. In contrast, the slope of 2.58 confirmed the significant net N_2O consumption in the ODZ core. Thereby the N_2O concentration simultaneously decreased to 0 at the middle of ODZ core (Fig. 1a). Furthermore, the isotopic composition of N_2O in the ODZ core is significantly different from that in the source layer, further ruling out vertical exchange with the source layer. Therefore, the long-term and large-scale anaerobic areas ensure net N_2O consumption in the ODZ core, which acts as the sink of N_2O . In other oceans, the N_2O peak was also observed at the lowest point of oxygen (Supplementary Fig. 6–11), although the boundary DO ranged from $10 \mu\text{M}$ to more than $300 \mu\text{M}$ (Fig. 1c). In the vast North Pacific Ocean and equatorial regions, the boundary DO is less than $50 \mu\text{M}$, accompanied by a shallow boundary depth (less than 1000 m), favouring excessive N_2O production and emission. A deeper source–

sink boundary has been found in the North Atlantic and Southern Oceans. The boundary DO increased to more than $300 \mu\text{M}$ with the boundary depth reaching 2000 m. Overall, the source–sink boundary of N_2O in the ocean was identified (Fig. 1), and the water column below the source–sink boundary does not contribute to atmospheric emissions; therefore, it was excluded from the remainder of this study.

Microbial processes governing N_2O production and consumption

To quantify the microbial sources of N_2O and the fraction of residual unreduced N_2O ($r_{\text{N}_2\text{O}}$) in the source part, the isotopic N_2O values obtained from Keeling plot (Supplementary Figs. 13–22), the corrected isotope signatures of the microbial sources (Supplementary Table 1–2), and the isotopic fractionation constants (i.e., ϵ_{N} : -15.4 ± 4.7 , ϵ_{O} : -7.1 ± 2.1 , and ϵ_{SP} : -5.9 ± 1.4) for N_2O reduction process were input to the model FRAME (Supplementary Fig. 23). In this study, four common microbial sources (HDN, NDN, AOB, AOA) and $r_{\text{N}_2\text{O}}$ was quantified (Supplementary Fig. 24, Supplementary Table 3). The linear regression relationships between N_2O microbial sources and boundary DO were uniformly adopted for extrapolation to global oceans (Supplementary Fig. 25, Fig. 2).

The primary productivity, substrate availability, boundary depth, and DO together determine the niche distribution of each N-cycling microorganism in the ocean. AOA dominate the nitrification pathway, contributing 34.1% of the N_2O in the ocean (Table 1), which is the dominant N_2O production pathway in the North Atlantic and Southern Oceans. Although both of them are chemoautotrophic processes, AOA have a greater affinity for NH_4^+ and oxygen^{20,22,27}. Thereby, AOA exceeds AOB in NH_4^+ -limited oceans with sharp oxyclines, while the contribution of AOB increases in high-latitude regions with high-oxygen (e.g., the Arctic Ocean and Antarctic Oceans). The isotopic signatures of N_2O in the Arctic Ocean have proved the important role of both AOA and AOB to N_2O productions¹². In the ODZs, AOB are completely depleted (2.2%) because of phytoplankton competition, rapidly decreasing oxygen gradients, and surface light inhibition derived from shallow boundary depths. HDN, fueled by organic matter exported from the photic zone, is the dominant N_2O production pathway in the North Pacific Ocean and equatorial regions. It further increases to 63.3% in ODZs because the abundant organic electron donors and sharp oxyclines create favorable conditions for incomplete denitrification. Notably, the contribution of denitrification is still considerable even if DO does not reach the anaerobic level in the open ocean. It is possibly associated with organic particles; the interior of sinking particles can afford a low-DO microenvironment²⁰. On a global scale (Fig. 2), the contribution of denitrification (HDN + NDN) to N_2O emissions is 61.1% (Table 1), nearly two-fold greater than that of nitrification (AOA + AOB). HDN is the first contributor to oceanic N_2O emission, whereas AOA are the most widely distributed contributor in the ocean.

Global distribution of N_2O flux in the ocean

To obtain the global N_2O flux in a year scale ($\text{Tg N}_2\text{O-N/yr}$), we first calculated the N_2O emissions by AOA ($\text{N}_2\text{O}_{\text{AOA}}$) in each grid on the basis of the ammonification flux (ammonia oxidation amount in a year scale), N_2O yield during ammonification ($\text{N}_2\text{O-N}/\text{NH}_4^+\text{-N}$), and the fraction of residual unreduced N_2O ($r_{\text{N}_2\text{O}}$, Supplementary Fig. 25e). The total N_2O flux was then obtained according to its proportion to total production in each grid (e.g., $\text{N}_2\text{O}_{\text{AOA}}/f_{\text{AOA}}$; see Methods for details). It is worth noting that the fraction of residual unreduced N_2O ($r_{\text{N}_2\text{O}}$) determines the net emission of N_2O . We established the empirical formula between the $r_{\text{N}_2\text{O}}$ and the boundary DO (Supplementary Fig. 25e). As the boundary DO rises, there is initially an increase in $r_{\text{N}_2\text{O}}$, followed by a subsequent decline. In ODZs with micro-oxic environment, the N_2O production and reduction are both active. As the boundary DO increases, the N_2O reduction is prior to be inhibited as

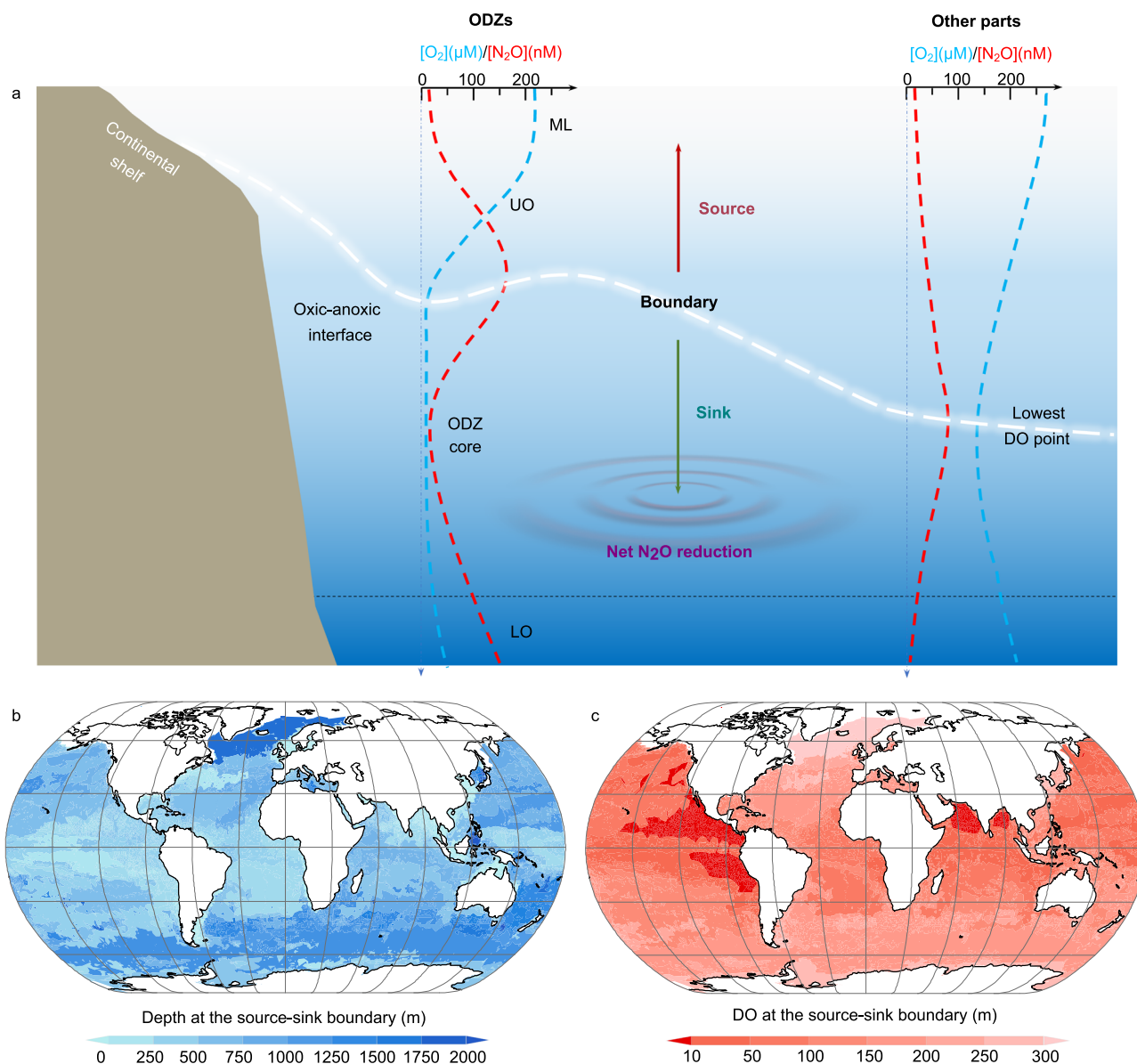


Fig. 1 | N_2O emission mechanism in the ocean. **a** The simultaneous changes in DO and N_2O in the ocean are represented by blue and red dotted lines. The source–sink boundary of N_2O , where N_2O reaches its highest value and below which the water column does not contribute to N_2O emissions, is identified by a comprehensive grid-by-grid (0.1°) traversal of DO up to 5000 m in the ocean. The areas with minimum $\text{O}_2 \leq 10 \mu\text{M}$ are defined as oxygen-deficient zones (ODZs), comprising a mixed layer (ML), upper oxycline (UO), ODZ core (OC), and lower oxycline (LO).

The DO generally remains stable ($> 200 \mu\text{M}$) in the ML and sharply decreases to zero in the UO; while it remains the lowest ($\text{O}_2 \leq 10 \mu\text{M}$) in the ODZ core and then increases from the LO. The oxic-anoxic interface occurs at the source–sink boundary in ODZs. **b, c** The distribution of depth and DO at the source–sink boundary of N_2O , which was identified at the lowest point of oxygen. Source data are provided as a Source Data file.

nitrous oxide reductase (nos) is the most O_2 sensitive denitrifying enzyme²⁸, leading to the increase of $r_{\text{N}_2\text{O}}$. However, the data obtained in the shallow Arctic Ocean and off the coast of Antarctica gave $r_{\text{N}_2\text{O}}$ values as low as 20% in spite of high boundary DO (Supplementary Fig. 25e)^{3,12,29}. This implies that a significant portion of the N_2O produced in situ or diffused from the atmosphere is reduced by denitrification in sediments¹².

The annual N_2O flux is 2.9 Tg/yr $\text{N-N}_2\text{O}$ (Fig. 3, Table 1), the distribution of which is in line with primary production pulses. On average, the turnover rate of phytoplankton (growth, death, and mineralization) is 45 times a year³⁰, providing never-ending NH_4^+ , NO_3^- , and organic matter for the continuous production of N_2O via nitrification and denitrification. Furthermore, the decay of phytoplankton creates the anaerobic environment for the significant production of

N_2O . Therefore, the oceans around the equator contribute the most to marine N_2O emissions, where ODZs disproportionately account for more than half of N_2O emissions (1.6 Tg $\text{N-N}_2\text{O}$) with only 0.1–0.2% of the ocean volume³¹. A higher flux of N_2O has also been observed in other oceans with high primary productivity, e.g., the Gulf of Guinea, Bay of Bengal, Gulf of Mexico, and Indonesia. In contrast, slight supersaturation and occasional undersaturation are predicted in the open Arctic Ocean and Southern Ocean, with limits on light and temperature at high latitudes. With respect to microbial sources (Table 1), the contribution of denitrification is almost twofold greater than that of nitrification. Traditional HDN is the largest contributor (1.6 Tg) to N_2O emissions in the ocean, which mainly occurs in ODZs (1.0 Tg). AOA are the most widely distributed contributors (1.0 Tg) in the NH_4^+ -limited ocean and completely overcome AOB (0.1 Tg) to N_2O emissions.

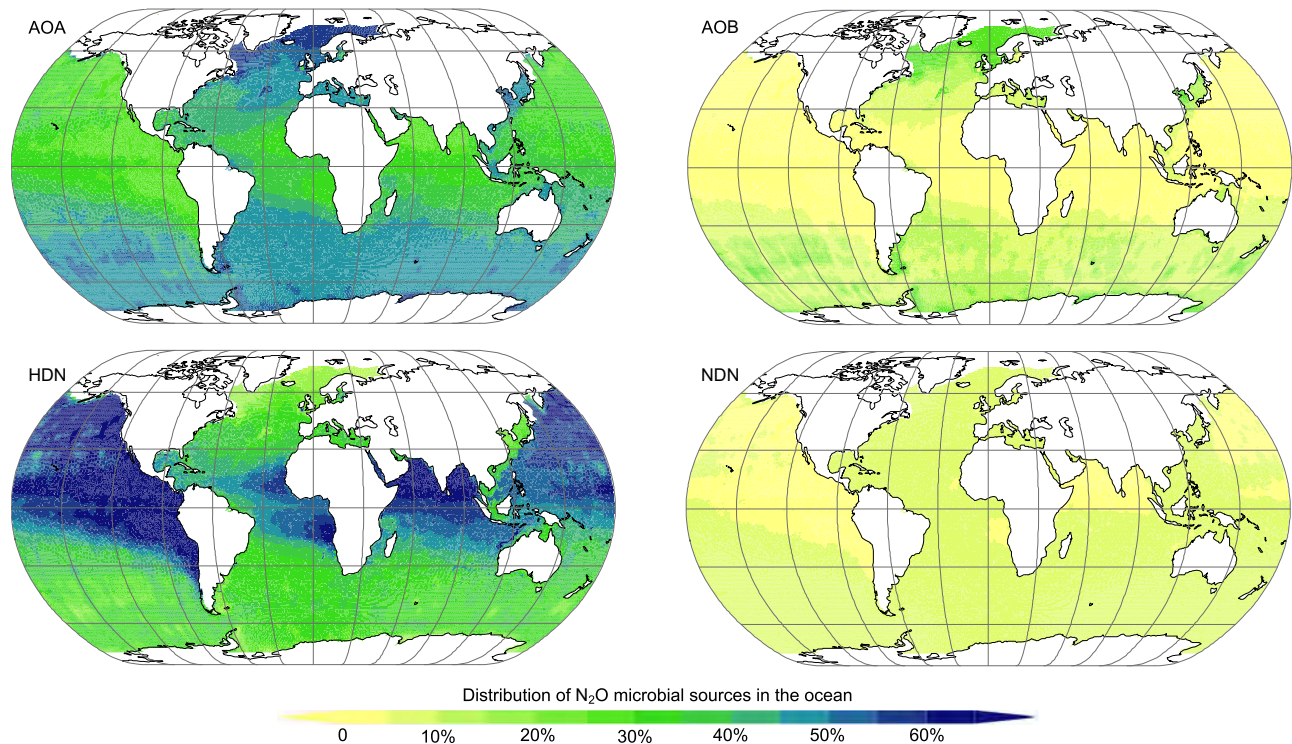


Fig. 2 | The spatial distribution of N₂O microbial sources (f_n , n = AOA, AOB, HDN, and NDN) in the ocean. The linear relationships between microbial sources and boundary DO were adopted for extrapolation to the global scale (Supplementary Fig. 25a-d). Additionally, a nonlinear relationship for AOB was also applied

in the extrapolation (Supplementary Fig. 26). Abbreviations: ammonia-oxidizing archaea (AOA), ammonia-oxidizing bacteria (AOB), nitrifier denitrification (NDN), heterotrophic denitrification (HDN). Source data are provided as a Source Data file.

The niche separation driven by primary productivity, substrate availability, boundary depth and DO, finally determines the N₂O emission patterns and flux in different marine habitats. Therefore, future ODZ expansion³² will certainly result in more N₂O emissions, while a decline in global primary production^{7,8} inversely reduces N₂O emissions. Whether N₂O flux increases is still an open question, which must be closely monitored, especially in the ODZ areas. More importantly, sporadic ODZs and widespread hypoxia have been observed in the North Pacific. As frigid waters become warmer with global warming, carbon fixation and the nitrogen cycle accelerate³⁰, potentially shoaling the source–sink boundary and forming new ODZs with subsequent N₂O hotspots. Additionally, it has been reported that the increase in N₂O emissions has not corresponded with external inputs in recent decades³³. In fact, the internal N cycle played a far more important role in N₂O production than did external inputs because of its large contribution to ammonification flux and organic matter. Therefore, coastal emissions are not comparable to those of naturally occurring ODZ areas in the ocean⁴.

Our results agree with previous estimations (Supplementary Table 4) from ocean biogeochemistry models^{4,6,9,10} but are slightly lower than those from empirical based methods and surface ocean

data^{3,34}. Our model considers the major microbial sources of N₂O, but several microbial or chemical processes, e.g., autotrophic denitrification or chemical denitrification^{35,36}, have not been integrated into the model. More efforts need to be made in cultivation to obtain comprehensive and accurate values of the isotopic characteristics of N₂O sources. Additionally, more in situ isotope measurements are necessary to constrain the highly variable relationship between microbial activity and boundary DO, so as to improve the accuracy of the extrapolation. Our static model might also underestimate the impact of upwelling, where coastal upwelling flux brings bottom water to the surface, a large amount of N₂O that should have been reduced is eventually released into the atmosphere²². Although some deficits exist in this model, its reliability has been confirmed by a large compilation (approximately 150,000) of N₂O in situ measurements at the global scale (Supplementary Fig. 28, $R^2 = 0.51$, in quantiles)³. For example, the N₂O emissions from three major ODZs are significant. The Pacific Ocean, in particular, has a symmetrical triangular emission distribution. The measured values agree with the predicted values for other regions with high productivity, such as the Gulf of Guinea, Bay of Bengal, and Indonesia. Some details, such as significant emissions in the Baltic and North Pacific Oceans and weak emissions in the North Atlantic, further confirm our results. Our study highlights the important role of the N₂O source–sink boundary and quantified microbial sources in the estimation of marine N₂O. This new framework will deepen our understanding of the oceanic N₂O emission mechanism from the bottom up. More importantly, it can be further refined with more observations to better characterize and predict the spatio-temporal dynamics of oceanic N₂O under a changing climate.

Methods

Data introduction

A literature search was conducted via bibliographic databases (e.g., Web of Science, Google Scholar, etc.) for papers containing N₂O and its

Table 1 | Microbial contribution (%) to N₂O emissions and N₂O flux (Tg N₂O-N/yr) in the ocean

Zones	Microbial contribution (%)				N ₂ O flux (Tg N ₂ O-N/yr)				Total
	AOA	AOB	HDN	NDN	AOA	AOB	HDN	NDN	
Global oceans	34.1	4.8	56.1	5.0	1.0	0.1	1.6	0.1	2.9
ODZs	29.8	2.2	63.3	4.7	0.5	0.03	1.0	0.1	1.6
other parts	39.4	8.1	47.2	5.4	0.5	0.1	0.6	0.1	1.3

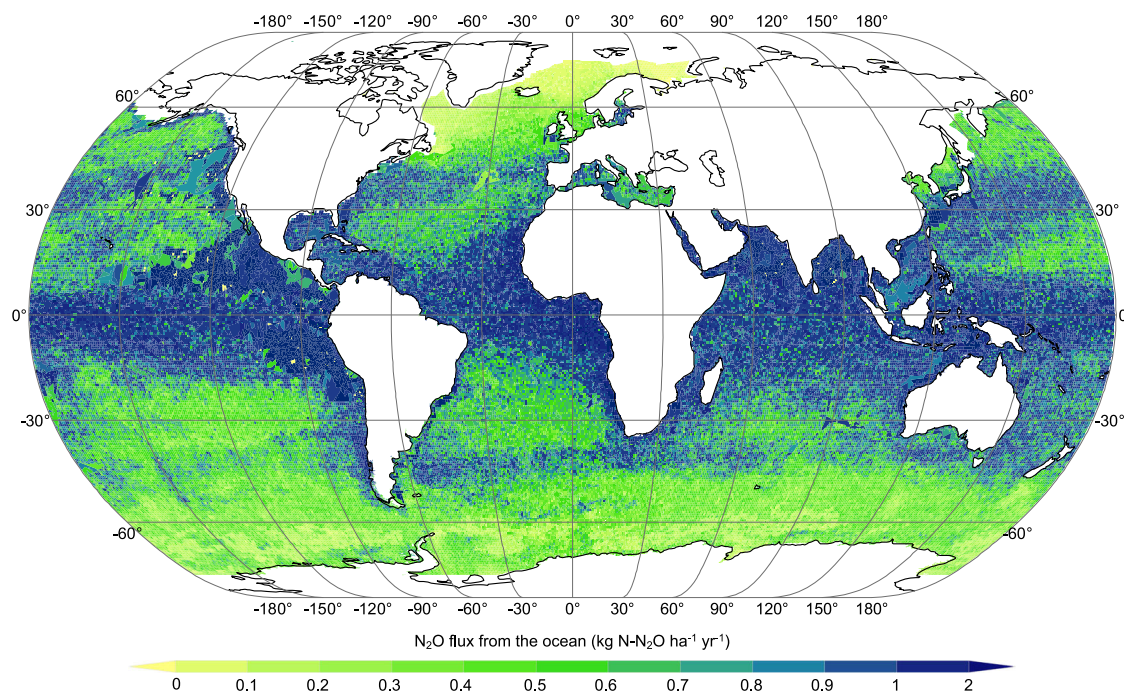


Fig. 3 | Global distribution of N_2O flux ($\text{kg N-N}_2\text{O ha}^{-1} \text{yr}^{-1}$) in the ocean. The global oceanic N_2O flux is $2.9 \text{ Tg N}_2\text{O-N/yr}$, which was calculated by AOA-produced N_2O flux and its proportion to total amount in each grid ($\text{N}_2\text{O}_{\text{AOA}}/f_{\text{AOA}}$). Source data are provided as a Source Data file.

isotope data from oceans (2000–2024). Data compilations were restricted to journal articles where the $\delta^{15}\text{N}^{\text{Bulk}}$, $\delta^{18}\text{O}$, and $\delta^{15}\text{N}^{\text{SP}}$ values of N_2O are available. Isotopomer ratios of a sample (R_{sample}) are expressed as per mil deviation from $^{15}\text{N}/^{14}\text{N}$ and $^{18}\text{O}/^{16}\text{O}$ ratios of the reference materials ($R_{\text{reference}}$), atmospheric N_2 , and standard mean ocean water (SMOW), respectively. $\delta^{15}\text{N}^{\text{Bulk}} = [(^{15}\text{N}/^{14}\text{N})_{\text{sample}} / (^{15}\text{N}/^{14}\text{N})_{\text{reference}} - 1] \times 1000\text{‰}$; $\delta^{18}\text{O} = [(^{18}\text{O}/^{16}\text{O})_{\text{sample}} / (^{18}\text{O}/^{16}\text{O})_{\text{reference}} - 1] \times 1000\text{‰}$. The ^{15}N site preference ($\delta^{15}\text{N}^{\text{SP}}$) is the difference in isotopic ^{15}N content between the central (α position) and the terminal N atom (β position) in the asymmetric N_2O molecule²¹, where $\delta^{15}\text{N}^{\text{Bulk}} = (\delta^{15}\text{N}^{\alpha} + \delta^{15}\text{N}^{\beta})/2$, $\delta^{15}\text{N}^{\alpha} = [^{14}\text{N}^{15}\text{N}^{16}\text{O}] / [^{14}\text{N}^{14}\text{N}^{16}\text{O}]$, $\delta^{15}\text{N}^{\beta} = [^{15}\text{N}^{14}\text{N}^{16}\text{O}] / [^{14}\text{N}^{14}\text{N}^{16}\text{O}]$, $\delta^{15}\text{N}^{\text{SP}} = \delta^{15}\text{N}^{\alpha} - \delta^{15}\text{N}^{\beta}$. Only field observations were collected, and simulations in the laboratory were excluded. In total, our efforts identified approximately 1000 lines of marine data with geochemical profiles of DO and N_2O concentrations and isotopic signatures ($\delta^{15}\text{N}^{\text{Bulk}}$, $\delta^{18}\text{O}$ and $\delta^{15}\text{N}^{\text{SP}}$, Supplementary Fig. 1–11). The raw data are available in the Supplementary Data 1.

Source–sink boundary of N_2O

According to the geochemical profiles of DO and N_2O concentration (Supplementary Figs. 2–11), N_2O exhibited a perfect mirror-image relationship with DO and reached its highest value at the lowest point of oxygen in oxygen-stratified oceans^{11,22}. The lowest point of oxygen is defined as the source–sink boundary of N_2O . The water column above the boundary was identified as the source; below it, the water column did not contribute to N_2O emissions due to the significant reduction of N_2O and acted as a N_2O sink. Due to drastic changes in DO in the ocean, the boundary values of DO and depth evolve synchronously in different marine habitats. Therefore, explaining the emission mechanism of N_2O at a fixed depth is difficult. Along the direction of the concentration gradient, a comprehensive grid-by-grid (1°) traversal of DO up to 5000 m was conducted globally to determine the depth where oxygen reached the lowest point in each grid (World Ocean Atlas, <https://www.noaa.gov/products/world-ocean-atlas>). With a resolution of over a million grids being traversed, the distribution and

depth of the source part were finally determined. The areas with minimum $\text{O}_2 \leq 10 \mu\text{M}$ are defined as ODZs (Supplementary Fig. 1, Supplementary Figs. 2–5), which consist of a mixed layer (ML), upper oxycline (UO), ODZ core (OC), and lower oxycline (LO). In other oceans, the N_2O peak was also observed at the lowest point of oxygen (Supplementary Fig. 1, Supplementary Fig. 6–11), although the boundary DO ranges from $10 \mu\text{M}$ to more than $300 \mu\text{M}$.

Keeling plot analyses

Each microbial process contributes differently to N_2O in the ocean, thereby leading to differences in the in situ N_2O isotopic signatures (i.e., $\delta^{15}\text{N}^{\text{Bulk}}$, $\delta^{18}\text{O}$, and $\delta^{15}\text{N}^{\text{SP}}$). However, the exchange of N_2O across air–water boundaries alters the microbial isotopic signatures of N_2O in the ocean^{13,37}. To avoid bias derived from atmosphere–water exchange, Keeling plot analyses were applied to obtain the microbial isotopic signatures of N_2O ³⁸. It assumes that the observed isotopic compositions is a mixture of atmospheric background values and the contributions from in situ microbial activity (Eq. 1–3), if the N_2O produced by the microbial processes have a constant signature throughout the water column of interest. Under this assumption of simple two-end member mixing, the isotopic composition of microbially produced N_2O is represented as the y-intercept value in the source part (Supplementary Fig. 13–22). It is worth noting that the atmosphere–water exchange was neglected for coastal waters because of the influence of upwelling¹³. Keeling plot analysis was also unsuitable for the ODZ core, as N_2O consumption other than mixing is the dominant process in this zone¹³.

$$[\text{N}_2\text{O}_{\text{observed}}] = [\text{N}_2\text{O}_{\text{atmosphere}}] + [\text{N}_2\text{O}_{\text{microbial}}] \quad (1)$$

$$\delta_{\text{observed}} * [\text{N}_2\text{O}_{\text{observed}}] = \delta_{\text{atmosphere}} * [\text{N}_2\text{O}_{\text{atmosphere}}] + \delta_{\text{microbial}} * [\text{N}_2\text{O}_{\text{microbial}}] \quad (2)$$

$$\delta_{\text{observed}} = \frac{1}{[\text{N}_2\text{O}]_{\text{observed}}} * (\delta_{\text{atmosphere}} - \delta_{\text{microbial}}) * [\text{N}_2\text{O}_{\text{atmosphere}}] + \delta_{\text{microbial}} \quad (3)$$

where $[N_2O]$ represents nitrous oxide concentration (nM) and δ is the isotopic composition (either $\delta^{15}N^{bulk}$, $\delta^{18}O-N_2O$, or $\delta^{15}N^{SP}$), and the subscripts indicate whether the observed signal is from atmosphere or microbial N_2O .

Microbial source partitioning by FRAME

N_2O microbial sources can be quantified by distributing in situ isotopic signatures to each microbial process^{38,39}. The software for the stable isotope Fractionation and Mixing Evaluation (FRAME, mal-ewick.github.io/frame) has been developed for simultaneous sources partitioning and fractionation progress determination¹⁹. Importantly, N_2O may undergo reduction processes, which can significantly alter their original isotopic signatures⁴⁰. During reduction, the $\delta^{15}N^{bulk}$, $\delta^{18}O$ and $\delta^{15}N^{SP}$ values of N_2O in unreacted N_2O increase with the isotopic fractionation constants⁴¹. Hence, the source partitioning should be combined with the potential isotopic fractionation of N_2O during its reduction to N_2 . In this study, the isotopic N_2O values obtained from Keeling plot, the corrected isotope signatures of the microbial sources, and the isotopic fractionation constants (i.e., ϵ_N : -15.4 ± 4.7 , ϵ_O : -7.1 ± 2.1 , and ϵ_{SP} : -5.9 ± 1.4) for N_2O reduction process were input to the model. As $\delta^{15}N^{bulk}$ and $\delta^{18}O$ are dependent on the substrates, exchange of O-isotopes between H_2O and precursors of N_2O also perturbs $\delta^{18}O$ of N_2O , we adopted corrected isotopic values to avoid bias from precursor substances^{19,40–42}. The precursor isotopic signatures ($\delta^{15}N-PON$, $\delta^{15}N-NO_3^-$, and $\delta^{18}O-H_2O$) were taken into account in FRAME^{13,44}. Because it is rare to obtain the isotopic values of NH_4^+ due to its low concentrations in oceans, the nitrogen isotope of particulate organic nitrogen (PON) minus the isotope effect (ϵ_{miner} , approximately -1%) was used as the background isotope value of ammonia³⁹. ϵ_{miner} is the isotope effect of nitrogen during the mineralization of phytoplankton. The $\epsilon^{15}N^{bulk}$, $\epsilon^{18}O$, and $\delta^{15}N^{SP}$ values of N_2O for each process and substrates of N_2O (PON, NO_3^- , or H_2O) were found in the literature (Supplementary Table 1-2). These values are obtained from common nitrifiers and denitrifiers, which have been widely used in the N_2O source partitioning of ocean and inland waters^{22,39,43,44}. The literature values are given as isotope effects ($\epsilon^{15}N^{bulk}$, $\epsilon^{18}O$), $\epsilon_{N_2O/precursor} = \delta_{N_2O} - \delta_{precursor}$. The input endmember values are corrected with the actually measured precursor values, $\delta_{N_2O_endmember} = \epsilon_{N_2O/precursor} + \delta_{actual_precursor}$. Specifically, the corrected $\delta^{15}N^{bulk}$ (‰) endmember values for AOA, AOB, and NDN depend on the value of $\delta^{15}N-PON + \epsilon_{miner}$, whereas $\delta^{15}N^{bulk}$ (‰) for HDN depends on the value of $\delta^{15}N-NO_3^-$. The $\delta^{18}O$ endmember values for HDN and NDN depend on the $\delta^{18}O-H_2O$. The actual isotopic signatures of the substrate in each region are summarized in Supplementary Table 2.

The contributions from the four major processes, ammonia-oxidizing by archaea (AOA), ammonia-oxidizing by bacteria (AOB), nitrifier denitrification (NDN), and heterotrophic denitrification (HDN) to N_2O production, and the degree of N_2O reduction were analyzed using the Monte Carlo modeling tool FRAME¹⁹. Importantly, fungal denitrifiers are not considered in this study, which generally play significant roles in acidic environments and are rarely detected in alkaline oceans⁴⁵. For now, we can get the quantified microbial sources (f_n , $n = HDN, NDN, AOB, AOA$) and the fraction of residual unreduced N_2O (r_{N_2O}). The detailed and step-by-step calculation can be found in the Supplementary Informations.

Ammonia-oxidation-based isotopic model for global N_2O estimation

In oceans, ammonia oxidation is performed mainly by AOA and AOB:

$$[NH_4^+] \times F_{AOA} \times Y_{AOA} \times r_{N_2O} : [NH_4^+] \times F_{AOB} \times Y_{AOB} \times r_{N_2O} = f_{AOA} : f_{AOB} \quad (4)$$

where $[NH_4^+]$ is the ammonia oxidation amount, F is the proportion of ammonia oxidation by AOA or AOB ($F_{AOB} + F_{AOA} = 1$), Y is the N_2O yield,

the average N_2O yield for AOA is 0.062% (0.019%, 0.089%), and that for AOB is 0.124% (0.075%, 0.180%) in the ocean (Supplementary Fig. 27)^{46–53}; r_{N_2O} is the fraction of residual unreduced N_2O ; f_n ($n = HDN, NDN, AOB$ and AOA) is the quantified microbial source of N_2O obtained via the FRAME.

As $F_{AOB} + F_{AOA} = 1$, we obtain:

$$F_{AOA} = \frac{1}{1 + \frac{Y_{AOA} f_{AOB}}{Y_{AOB} f_{AOA}}} \quad (5)$$

$$F_{AOB} = \frac{1}{1 + \frac{Y_{AOB} f_{AOA}}{Y_{AOA} f_{AOB}}} \quad (6)$$

Now, we can obtain the N_2O amount produced by AOA and finally calculate the total amount of N_2O emissions.

$$N_2O_{AOA} = [NH_4^+] \times F_{AOA} \times Y_{AOA} \times r_{N_2O} \quad (7)$$

$$N_2O_{total} = [NH_4^+] \times F_{AOA} \times Y_{AOA} \div f_{AOA} \times r_{N_2O} \quad (8)$$

Once the N_2O emissions from AOA have been calculated on the basis of the ammonia oxidation amount $[NH_4^+]$, the proportion of ammonia oxidation by AOA (F_{AOA}), the N_2O yield (Y_{AOA}), and the fraction of residual unreduced N_2O (r_{N_2O}), the total N_2O emission can be obtained according to its contribution to the total emissions f_{AOA} . The next step is to estimate the amount of ammonia oxidation in each grid (1°) of marine systems. Generally, nitrate accounts for as much as 88% of the dissolved inorganic nitrogen (NH_4^+ , NO_2^- , and NO_3^-) pool, and ammonium remains at low levels or even below detection limits⁵⁴. Whenever NH_4^+ is input or produced, it is oxidized or assimilated immediately. That is: ammonification amount = the external input of NH_4^+ + the mineralization of organic-N - the amount of NH_4^+ assimilated by phytoplankton. The organic-N are mainly derived from the external input (NH_4^+ and organic-N) and the phytoplankton assimilation (from NH_4^+ and NO_3^-). Therefore, the annual ammonification amount equals the sum of the external input and the phytoplankton assimilation from NO_3^- in a year scale. In other words, when NH_4^+ is assimilated by phytoplankton, it doesn't experience the ammonification process. Thereby we didn't account for assimilation of NH_4^+ by primary producers.

The external inputs of ammonia, including atmospheric N deposition⁵⁵, ammonia volatilization⁵⁶, nitrogen fixation⁵⁷, and terrestrial N inputs (from rivers⁵⁷ and groundwater⁵⁸), were integrated to estimate ammonia oxidation. Specifically, atmospheric N deposition, including rainfall and dust fall, transports considerable quantities of nitrogen compounds into the ocean. Ammonia also escapes from surface water to the atmosphere, which is particularly significant in shallow and warm waters. Nitrogen fixation could increase the amount of N available in the ocean, particularly in oligotrophic waters. Affected by agricultural runoff, industrial discharge, and domestic sewage, rivers and groundwater also increase the nitrogen concentration in coastal waters. These processes directly impact the marine nitrogen cycle, increasing the potential substrate for ammonia oxidation.

In addition to external inputs, the internal N cycle also plays a key role. The growth, death and mineralization of phytoplankton provide never-ending NH_4^+ , NO_3^- , and organic matter for the continuous production of N_2O . The net primary productivity (NPP) is calculated from available dataset⁵⁹. As phytoplankton take up nutrients at an average ratio of approximately 106 C:16 N:1 P (Redfield ratio)⁶⁰, we can obtain the organic nitrogen produced from the NPP. The so-called Redfield ratio is the stoichiometric ratio of essential elements in average phytoplankton biomass. Subsequently, the phytoplankton assimilation amount from nitrate was obtained based on the absorb ratio of NH_4^+ /

($\text{NH}_4^+ + \text{NO}_3^-$) in specific areas⁶¹. Considering the efficiency of mineralization (70%) and sedimentation (15%) of organic matter to the deep sea^{30,62}, the amount of internal ammonia was ultimately obtained. The detailed method for the calculation of primary productivity is represented by the following equation:

$$\frac{\partial P(x, t)}{\partial t} = dr \cdot \nabla^2 P(x, t) + cP \cdot NPP(x, t) - dec \cdot P(x, t) \quad (9)$$

where $P(x, t)$ denotes the primary productivity varying with space x and time t . The operator ∇^2 is the Laplacian, which represents the second spatial derivative. dr represents the diffusion rate of primary productivity in space⁶³, cP represents the contribution of NPP to primary productivity⁶⁴, dec represents the natural decay of primary productivity over time⁶⁵, and the photosynthesis and respiration processes were simulated for each grid based on environmental parameters such as light and temperature, which decrease with ocean depth. These coefficients are calibrated via heuristic algorithms. Depending on the specific problem, either Dirichlet boundary conditions (fixed boundary values) or Neumann boundary conditions (fixed boundary derivatives) can be chosen⁶⁶.

In this specific calculation, we used a three-dimensional grid to represent the marine environment, and each grid (0.1°) represented a sea area with a specific depth. The basic parameters, e.g., water temperature⁶⁷, pH⁶⁸, salinity⁶⁹, and oxygen⁷⁰, were input, along with the external and internal inputs. The XGBoost algorithm-based downscaling approach was applied to enhance the spatial resolution. The calculated depth was determined on the basis of the source–sink boundary of N_2O , with the boundary depth ranging from approximately 300 m in the ODZs to 2000 m in other oceans. As depth increased, the oxygen content, light intensity, temperature, salinity, and primary productivity exhibited dynamic changes that significantly impacted the microorganisms' metabolic rate and ammonia oxidation process. The reaction rate was adjusted to ensure that the model could accurately reflect the ammonia oxidation process at different depths and under different oxygen conditions. Further details for specific formulas and parameters are available in the Supplementary Informations and the Supplementary Code 1.

Data availability

The data generated in this study are provided in the Supplementary Data 1. Source data are provided with this paper.

Code availability

The codes of this study are available in Supplementary Code 1.

References

- Greenhouse Gas Bulletin. <https://public.wmo.int/en/greenhouse-gas-bulletin> (2022).
- Prather, M. J. et al. Measuring and modeling the lifetime of nitrous oxide including its variability. *J. Geophys. Res. Atmos.* **120**, 5693–5705 (2015).
- Yang, S. et al. Global reconstruction reduces the uncertainty of oceanic nitrous oxide emissions and reveals a vigorous seasonal cycle. *Proc. Natl. Acad. Sci.* **117**, 11954–11960 (2020).
- Tian, H. et al. A comprehensive quantification of global nitrous oxide sources and sinks. *Nature* **586**, 248–256 (2020).
- Rhee, T. S., Kettle, A. J. & Andreae, M. O. Methane and nitrous oxide emissions from the ocean: A reassessment using basin-wide observations in the Atlantic. *J. Geophys. Res. Atmos.* **114**, (2009).
- Buitenhuis, E. T., Suntharalingam, P. & Le Quéré, C. Constraints on global oceanic emissions of N_2O from observations and models. *Biogeosciences* **15**, 2161–2175 (2018).
- Landolfi, A., Somes, C. J., Koeve, W., Zamora, L. M. & Oschlies, A. Oceanic nitrogen cycling and N_2O flux perturbations in the Anthropocene. *Glob. Biogeochem. Cycles* **31**, 1236–1255 (2017).
- Martinez-Rey, J., Bopp, L., Gehlen, M., Tagliabue, A. & Gruber, N. Projections of oceanic N_2O emissions in the 21st century using the IPSL Earth system model. *Biogeosciences* **12**, 4133–4148 (2015).
- Battaglia, G. & Joos, F. Marine N_2O emissions from nitrification and denitrification constrained by modern observations and projected in multimillennial global warming simulations. *Glob. Biogeochem. Cycles* **32**, 92–121 (2018).
- Ji, Q., Buitenhuis, E., Suntharalingam, P., Sarmiento, J. L. & Ward, B. B. Global nitrous oxide production determined by oxygen sensitivity of nitrification and denitrification. *Glob. Biogeochem. Cycles* **32**, 1790–1802 (2018).
- Kelly, C. L., Travis, N. M., Baya, P. A. & Casciotti, K. L. Quantifying nitrous oxide cycling regimes in the Eastern Tropical North Pacific Ocean with isotopomer analysis. *Glob. Biogeochem. Cycles* **35**, e2020GB006637 (2021).
- Toyoda, S. et al. Distribution and production mechanisms of N_2O in the Western Arctic Ocean. *Glob. Biogeochem. Cycles* **35**, e2020GB006881 (2021).
- Casciotti, K. L. et al. Nitrous oxide cycling in the Eastern Tropical South Pacific as inferred from isotopic and isotopomeric data. *Deep Sea Res. Part II Top. Stud. Oceanogr.* **156**, 155–167 (2018).
- Breitbart, D. et al. Declining oxygen in the global ocean and coastal waters. *Science* **359**, eaam7240 (2018).
- Wuchter, C. et al. Archaeal nitrification in the ocean. *Proc. Natl. Acad. Sci.* **103**, 12317–12322 (2006).
- Martens-Habben, W., Berube, P. M., Urakawa, H., de la Torre, J. R. & Stahl, D. A. Ammonia oxidation kinetics determine niche separation of nitrifying Archaea and Bacteria. *Nature* **461**, 976–979 (2009).
- Bourbonnais, A. et al. N_2O production and consumption from stable isotopic and concentration data in the Peruvian coastal upwelling system. *Glob. Biogeochem. Cycles* **31**, 678–698 (2017).
- Tang, W. et al. Nitrous oxide production in the Chesapeake Bay. *Limnol. Oceanogr.* **12191** <https://doi.org/10.1002/lno.12191> (2022).
- Lewicki, M. P., Lewicka-Szczepak, D. & Skrzypek, G. FRAME—Monte Carlo model for evaluation of the stable isotope mixing and fractionation. *PLOS ONE* **17**, e0277204 (2022).
- Toyoda, S. et al. Extensive accumulation of nitrous oxide in the oxygen minimum zone in the Bay of Bengal. *Glob. Biogeochem. Cycles* **37**, e2022GB007689 (2023).
- Toyoda, S. et al. Production mechanism and global budget of N_2O inferred from its isotopomers in the western North Pacific. *Geophys. Res. Lett.* **29**, 7-1–7-4 (2002).
- Toyoda, S. et al. Identifying the origin of nitrous oxide dissolved in deep ocean by concentration and isotopocule analyses. *Sci. Rep.* **9**, 7790 (2019).
- Popp, B. N. et al. Nitrogen and oxygen isotopomeric constraints on the origins and sea-to-air flux of N_2O in the oligotrophic subtropical North Pacific gyre. *Glob. Biogeochem. Cycles* **16**, 12-1–12-10 (2002).
- Ostrom, N. E. et al. Isotopologue effects during N_2O reduction in soils and in pure cultures of denitrifiers. *J. Geophys. Res.* **112**, G02005 (2007).
- Jinuntuya-Nortman, M., Sutka, R. L., Ostrom, P. H., Gandhi, H. & Ostrom, N. E. Isotopologue fractionation during microbial reduction of N_2O within soil mesocosms as a function of water-filled pore space. *Soil Biol. Biochem.* **40**, 2273–2280 (2008).
- Yamagishi, H. et al. Role of nitrification and denitrification on the nitrous oxide cycle in the eastern tropical North Pacific and Gulf of California. *J. Geophys. Res. Biogeosci.* **112**, (2007).
- Liu, S. et al. Potential correlated environmental factors leading to the niche segregation of ammonia-oxidizing archaea and

- ammonia-oxidizing bacteria: a review. *Appl. Environ. Biotechnol.* **2**, 11–19 (2017).
28. Beaulieu, J. J. et al. Nitrous oxide emission from denitrification in stream and river networks. *Proc. Natl. Acad. Sci. USA* **108**, 214–219 (2011).
 29. Boontanon, N., Watanabe, S., Odate, T. & Yoshida, N. Production and consumption mechanisms of N₂O in the Southern Ocean revealed from its isotopomer ratios. *Biogeosci. Discuss* **7**, 7821–7848 (2010).
 30. Falkowski, P. Ocean Science: The power of plankton. *Nature* **483**, S17–S20 (2012).
 31. Zhang, I. H. et al. Partitioning of the denitrification pathway and other nitrite metabolisms within global oxygen deficient zones. *ISME Commun.* **3**, 1–14 (2023).
 32. Cabré, A., Marinov, I., Bernardello, R. & Bianchi, D. Oxygen minimum zones in the tropical Pacific across CMIP5 models: mean state differences and climate change trends. *Biogeosciences* **12**, 5429–5454 (2015).
 33. Thompson, R. L. et al. Acceleration of global N₂O emissions seen from two decades of atmospheric inversion. *Nat. Clim. Change* **9**, 993–998 (2019).
 34. Bianchi, D., Dunne, J. P., Sarmiento, J. L. & Galbraith, E. D. Data-based estimates of suboxia, denitrification, and N₂O production in the ocean and their sensitivities to dissolved O₂. *Glob. Biogeochem. Cycles* **26** (2012).
 35. Dalsgaard, T., De Brabandere, L. & Hall, P. O. J. Denitrification in the water column of the central Baltic Sea. *Geochim. Cosmochim. Acta* **106**, 247–260 (2013).
 36. Stanton, C. L. et al. Nitrous oxide from chemodenitrification: A possible missing link in the Proterozoic greenhouse and the evolution of aerobic respiration. *Geobiology* **16**, 597–609 (2018).
 37. Pataki, D. E. et al. The application and interpretation of Keeling plots in terrestrial carbon cycle research. *Glob. Biogeochem. Cycles* **17** (2003).
 38. Wang, S., Zhi, W., Li, S., Lyu, T. & Ji, G. Sustainable management of riverine N₂O emission baselines. *Natl. Sci. Rev.* **12**, nwae458 (2025).
 39. Yoshikawa, C. et al. Insight into nitrous oxide production processes in the western North Pacific based on a marine ecosystem isotopomer model. *J. Oceanogr.* **72**, 491–508 (2016).
 40. Wu, D. et al. Quantifying N₂O reduction to N₂ during denitrification in soils via isotopic mapping approach: Model evaluation and uncertainty analysis. *Environ. Res.* **179**, 108806 (2019).
 41. Lewicka-Szczebak, D., Lewicki, M. P. & Well, R. N₂O isotope approaches for source partitioning of N₂O production and estimation of N₂O reduction—validation with the ¹⁵N gas-flux method in laboratory and field studies. *Biogeosciences* **17**, 5513–5537 (2020).
 42. Rohe, L., Well, R. & Lewicka-Szczebak, D. Use of oxygen isotopes to differentiate between nitrous oxide produced by fungi or bacteria during denitrification. *Rapid Commun. Mass Spectrom.* **31**, 1297–1312 (2017).
 43. Liang, X. et al. Nitrification regulates the spatiotemporal variability of N₂O emissions in a Eutrophic Lake. *Environ. Sci. Technol.* <https://doi.org/10.1021/acs.est.2c03992>. (2022).
 44. Wang, S. et al. Long-neglected contribution of nitrification to N₂O emissions in the Yellow River. *Environ. Pollut.* **351**, 124099 (2024).
 45. Chen, X. et al. Tracing microbial production and consumption sources of N₂O in rivers on the Qinghai-Tibet Plateau via isotopocule and functional microbe analyses. *Environ. Sci. Technol.* **57**, 7196–7205 (2023).
 46. Hink, L., Nicol, G. W. & Prosser, J. I. Archaea produce lower yields of N₂O than bacteria during aerobic ammonia oxidation in soil. *Environ. Microbiol.* **19**, 4829–4837 (2017).
 47. Hink, L., Gubry-Rangin, C., Nicol, G. W. & Prosser, J. I. The consequences of niche and physiological differentiation of archaeal and bacterial ammonia oxidisers for nitrous oxide emissions. *ISME J.* **12**, 1084–1093 (2018).
 48. Jung, M.-Y. et al. Isotopic signatures of N₂O produced by ammonia-oxidizing archaea from soils. *ISME J.* **8**, 1115–1125 (2014).
 49. Jung, M.-Y. et al. Enrichment and characterization of an autotrophic ammonia-oxidizing archaeon of mesophilic crenarchaeal group I.1a from an agricultural soil. *Appl. Environ. Microbiol.* **77**, 8635–8647 (2011).
 50. Stieglmeier, M. et al. Aerobic nitrous oxide production through N-nitrosating hybrid formation in ammonia-oxidizing archaea. *ISME J.* **8**, 1135–1146 (2014).
 51. Qin, W. et al. Influence of oxygen availability on the activities of ammonia-oxidizing archaea. *Environ. Microbiol. Rep.* **9**, 250–256 (2017).
 52. Santoro, A. E., Buchwald, C., McIlvin, M. R. & Casciotti, K. L. Isotopic signature of N₂O produced by marine ammonia-oxidizing archaea. *Science* **333**, 1282–1285 (2011).
 53. Jiang, Q.-Q. & Bakken, L. R. Nitrous oxide production and methane oxidation by different ammonia-oxidizing bacteria. *Appl. Environ. Microbiol.* **65**, 2679–2684 (1999).
 54. Bristow, L. A., Mohr, W., Ahmerkamp, S. & Kuypers, M. M. M. Nutrients that limit growth in the ocean. *Curr. Biol.* **27**, R474–R478 (2017).
 55. Myriokefalitakis, S., Gröger, M., Hieronymus, J. & Döscher, R. An explicit estimate of the atmospheric nutrient impact on global oceanic productivity. *Ocean Sci.* **16**, 1183–1205 (2020).
 56. Paulot, F. et al. Global oceanic emission of ammonia: constraints from seawater and atmospheric observations. *Glob. Biogeochem. Cycles* **29**, 1165–1178 (2015).
 57. Wang, W.-L., Moore, J. K., Martiny, A. C. & Primeau, F. W. Convergent estimates of marine nitrogen fixation. *Nature* **566**, 205–211 (2019).
 58. Beusen, A. H. W., Slomp, C. P. & Bouwman, A. F. Global land–ocean linkage: direct inputs of nitrogen to coastal waters via submarine groundwater discharge. *Environ. Res. Lett.* **8**, 034035 (2013).
 59. Ocean Productivity: NPP Productivity Models. <https://sites.science.oregonstate.edu/ocean.productivity/vgpm.model.php>.
 60. Weber, T. S. & Deutsch, C. Ocean nutrient ratios governed by plankton biogeography. *Nature* **467**, 550–554 (2010).
 61. Dortch, Q. The interaction between ammonium and nitrate uptake in phytoplankton. *Mar. Ecol. Prog. Ser.* **61**, 183–201 (1990).
 62. Lin, X. et al. Gross nitrogen mineralization in surface sediments of the Yangtze Estuary. *PLOS ONE* **11**, e0151930 (2016).
 63. Aquatic Photosynthesis | Princeton University Press. <https://press.princeton.edu/books/paperback/978069115511/aquatic-photosynthesis> (2007).
 64. Eppley, R. W. & Peterson, B. J. Particulate organic matter flux and planktonic new production in the deep ocean. *Nature* **282**, 677–680 (1979).
 65. Oxygen minimum zones (OMZs) in the modern ocean. *Prog. Oceanogr.* **80**, 113–128 (2009).
 66. Capone, D. G. & Hutchins, D. A. Microbial biogeochemistry of coastal upwelling regimes in a changing ocean. *Nat. Geosci.* **6**, 711–717 (2013).
 67. Ocean Temperature. <http://app01.saeon.ac.za/sadcofunstuff/OceanTemperature.htm>.
 68. New Global Maps Detail Human-Caused Ocean Acidification—The Earth Institute—Columbia University. <https://www.earth.columbia.edu/articles/view/3211>.
 69. Olmedo, E. et al. Nine years of SMOS sea surface salinity global maps at the Barcelona Expert Center. *Earth Syst. Sci. Data* **13**, 857–888 (2021).
 70. World Ocean Atlas. National Centers for Environmental Information (NCEI) <https://www.ncei.noaa.gov/products/world-ocean-atlas> (2021).

Acknowledgements

This work was supported by the Key Projects of the Joint Fund of the National Natural Science Foundation of China (NSFC) (No. U22A20557), the National Natural Science Foundation of China (NSFC) (No. 52379084), the National Key Research and Development Program of China (No. 2022YFE0138300), and Yunnan Provincial Science and Technology Project at Southwest United Graduate School (No. 202302AO370015). Additionally, we would like to express our sincere appreciation to Dr. Sakae Toyoda for providing the N₂O datasets used in this study.

Author contributions

Conceptualization was carried out by G.D.J. and S.W. Investigation and visualization were carried out by S.W., J.L.H., and S.J.L. Original draft was written by S.W. Review and editing of the draft was carried out by Z.W., X.F.Z., Y.L., and G.D.J. Supervision was the responsibility of G.D.J. and Y.L.

Competing interests

The authors declare no competing interests.

Additional information

Supplementary information The online version contains supplementary material available at <https://doi.org/10.1038/s41467-025-58715-4>.

Correspondence and requests for materials should be addressed to Yong Liu or Guodong Ji.

Peer review information *Nature Communications* thanks Sushmita Deb, Dominika Lewicka-Szczebak, and the other anonymous reviewer(s) for their contribution to the peer review of this work. A peer review file is available.

Reprints and permissions information is available at <http://www.nature.com/reprints>

Publisher's note Springer Nature remains neutral with regard to jurisdictional claims in published maps and institutional affiliations.

Open Access This article is licensed under a Creative Commons Attribution-NonCommercial-NoDerivatives 4.0 International License, which permits any non-commercial use, sharing, distribution and reproduction in any medium or format, as long as you give appropriate credit to the original author(s) and the source, provide a link to the Creative Commons licence, and indicate if you modified the licensed material. You do not have permission under this licence to share adapted material derived from this article or parts of it. The images or other third party material in this article are included in the article's Creative Commons licence, unless indicated otherwise in a credit line to the material. If material is not included in the article's Creative Commons licence and your intended use is not permitted by statutory regulation or exceeds the permitted use, you will need to obtain permission directly from the copyright holder. To view a copy of this licence, visit <http://creativecommons.org/licenses/by-nc-nd/4.0/>.

© The Author(s) 2025